

# UNSTEADY FLOW STRUCTURES WITHIN A TURBINE RIM SEAL CAVITY IN THE PRESENCE OF PURGE FLOW

*"An Experimental and Computational Unsteady Aerodynamics Investigation"*

Cengiz Camci<sup>1</sup>

Michael Averbach<sup>2</sup>

Jason Town<sup>3</sup>

Department of Aerospace Engineering

The Pennsylvania State University, Turbomachinery Aero-heat Transfer Lab

University Park, Pennsylvania, USA

## ABSTRACT

## NOMENCLATURE

Flow within the space between the rotor and stator of a turbine disk, and an area referred to as the rim seal cavity, develops azimuthal velocity component from the rotor disk. The fluid within develops unsteady structures that move at a fraction of the rotor speed. A test is designed to measure the number of unsteady structures and the rotational speed at which they are moving in the rim seal cavity of an experimental research rig. Data manipulation was developed to extract the speed, and the numbers of structures present using two fast response aerodynamic probes measuring static pressure on the surface of the NGV-side rim seal cavity. A computational study is done to compare measured results to a transient URANS. The computational simulation consists of 8 vanes and 10 blades, carefully picked to reduce the error caused by blade vane pitch mismatch and to allow for the structures to develop correctly, and the rim seal cavity to measure the speed and number of the structures. The experimental results found 15 structures moving at 77.5% of the rotor speed, and the computational study suggested 14.5 structures are moving at 81.7% rotor speed. The agreement represents the first known test of its kind in a large-scale turbine test rig and the first known "good" agreement between computational and experimental work.

<sup>1</sup> Prof. of Aerospace Eng., ASME Fellow, Pennsylvania State University

<sup>2</sup> Presently at Bechtel Marine Propulsion Corp.

<sup>3</sup> Presently at Applied Research Lab., Pennsylvania State University

AFTRF	Axial Flow Turbine Research Facility
NGV	Nozzle Guide Vane
$\theta_{diff}$	Difference in degrees between transducers
$t_{phase}$	Difference in time between each peak across each transducer
$\omega_{rotor}$	Rotor speed in radians per second
$N_{str\ total}$	Total number of structures identified
$T_{sample}$	Total sample time in seconds
$\Omega_{str}$	Speed of the structure in radians per second
$f_{str}$	The frequency at which a structure passes by a transducer
$N_{str}$	Number of structures
$N_{str\ per\ second}$	Number of structures that pass by the transducer per second
$f^*$	Occurrences per rotor revolution
$f$	Frequency in Hertz
$\dot{m}_{purge}$	Mass flow rate injected into the rim seal cavity
$\dot{m}_{gaspath}$	Mass flow rate though the main gas path
$RPM_{rotor}$	Rotor speed in rotations per minute
T	Time to rotate the rotor one blade pitch
t	Elapsed time from start
$\theta_{peak,t}$	Peak location at time step
$\theta_{peak,t+1}$	Peak location at next time step
$\Delta t$	Computational time step

## INTRODUCTION

Design of a turbine stage requires a gap between the non-moving stator wall and the rotating blade disk below the hub endwall surface. Air within the rim seal cavity begins to swirl due to momentum imparted on the fluid through boundary layer interaction with the rotor disk. As the system of swirl develops, a system of high to low-pressure cells moves within the rim seal cavity. The cells are identified by Cao et al. in a computational and experimental study of a two-stage turbine [1]. The results conclude that eight unsteady structures are moving at 90% to 97% of the rotor speed. The structures present are independent of blade passing events.

Jakoby et al.[2] presented comparisons of three different types of computational studies. The test that best represents the structures within the rim seal cavity is a complete 360-degree analysis. The rim seal cavity produced three unsteady structures, and they are moving at 80% of the rotor speed. The geometry does not include the vanes or blades but simulates them by imposing static pressure fields as their boundaries.

A computational test done by Julien et al. [3] includes a sector model of a model with 44 inlet guide vanes and 58 rotor blades. The model shows about 30 structures within the rim seal cavity; they are moving at 90% of the rotor speed. A variety of purge injection rates in multiple tests showed that increasing the injection rate causes these structures to dissipate. The results are highly dependent on the design of the rim seal cavity.

A full unsteady 360-degree study based on the axial flow turbine test rig at Arizona State by Wang et al. [4] also has found evidence of the unsteady structures within the rim seal cavity. In this study, the structures are found to correspond with ingress and egress out of fluid from the mainstream to the rim seal cavity. There are 12 cells moving at 87% of the rotor speed. They also observed that the cells dissipate at higher purge flow rates. A criticism by Mirzamoghadam et al. was written claiming that the structures found may be a transient phenomenon that is caused by an insignificant number of revolutions of the rotor performed to resolve the case to a satisfactory solution [5].

The results concur that the cell size, shape, and speed are dependent on the design of the rim seal cavity and not the number of blades or vanes of the stage. A larger, more unobstructed cavity tends to lead toward larger pressure structures in smaller quantities that each take up greater azimuthal angles within the rim seal cavity. The current design is going toward smaller and more complex cavities than those tested by Cao and Jakoby et al. [2]. The new cavity designs have smaller and more numerous structures, each structure taking up a smaller azimuthal angle. These structures can be measured using fast response aerodynamic probes on the surface of the stator wall or the rotor disk, as Palafox et al. have done so [6]. They can also be simulated using a partial sector of the rim seal cavity if the sector is picked while keeping the number of structures in mind.

Basol et al. [7] at ETH Zurich studied a complete annulus solution by using a GPU powered URANS solver. Two different

cases based on experimental geometries were used. In the first case using a 0.4% injection rate, no unsteady structures were found. In the case with a higher injection rate (0.9% injection rate) a separation bubble was located inside the cavity. The separation gave rise to unsteady structures within the rim seal cavity.

Additionally, it was found that the magnitude of the sinusoidal static pressure distribution is more significant when a full 360° annular model than a model of 20° sector. Both models correctly predict the correct number of peaks and troughs. Palafox et. al. also made a computational effort for modeling hot gas ingestion in a 1.5-Stage Turbine Wheelspace Hot Gas Ingestion Rig (HGIR) [8].

The goal of this paper is to correctly measure the speed and number of unsteady structures within the rim seal cavity experimentally, using the Axial Flow Turbine Research Facility at The Pennsylvania State University. With reliable data from an experimental rig the next step is to use the results to guide our computational efforts. The ultimate goal is being able to predict and accurately reproduce measured unsteady structures within the experimental rig with a present computational URANS method.

## NOMENCLATURE

AFTRF	Axial Flow Turbine Research Facility
NGV	Nozzle Guide Vane
$\theta_{diff}$	Difference in degrees between transducers
$t_{phase}$	Difference in time between each peak across each transducer
$\omega_{rotor}$	Rotor speed in radians per second
$N_{str\ total}$	Total number of structures identified
$T_{sample}$	Total sample time in seconds
$\Omega_{str}$	Speed of the structure in radians per second
$f_{str}$	The frequency at which a structure passes by a transducer
$N_{str}$	Number of structures
$N_{str\ per\ second}$	Number of structures that pass by the transducer per second
$f^*$	Occurrences per rotor revolution
$f$	Frequency in Hertz
$\dot{m}_{purge}$	Mass flow rate injected into the rim seal cavity
$\dot{m}_{gaspath}$	Mass flow rate though the main gas path
$RPM_{rotor}$	Rotor speed in rotations per minute
$T$	Time to rotate the rotor one blade pitch
$t$	Elapsed time from start
$\theta_{peak,t}$	Peak location at time step
$\theta_{peak,t+1}$	Peak location at next time step
$\Delta t$	Computational time step

## EXPERIMENTAL SETUP

**Turbine Research Facility:** The current configuration of the Axial Flow Turbine Research Facility (AFTRF) has 29 Nozzle Guide Vanes and 36 blades in its rotor. It is a large scale

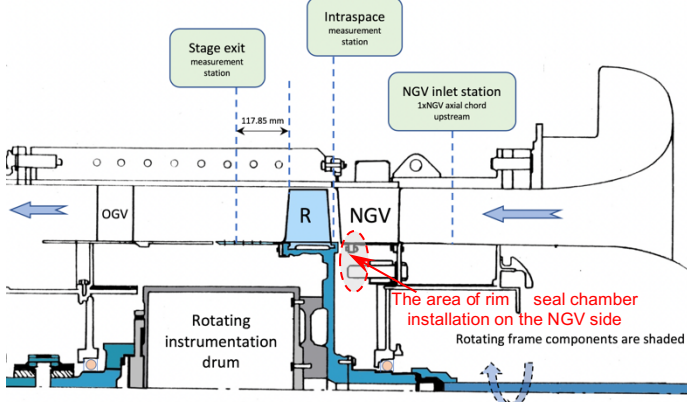


Figure 1 : Cross-sectional view of AFTRF

[0.916 m (36.08 inches)] diameter, long duration, low-speed turbine test stage that simulates state-of-the-art turbine blades, nozzle guide vanes, and rim seal cavity flows. A downstream, four stage axial flow fan system can provide the turbine with 40 inches of water (10000 Pa) pressure drop and a maximum flow rate of 10 kg/s.

The AFTRF as shown in Figure 1 is an open-circuit turbine rig of cold flow type with atmospheric inlet temperature and pressure. The bell-mouth type inlet of the facility is followed by the test section containing a single HP turbine stage. The rotor assembly generates around 80 HP of power with a typical temperature drop of 5 – 70 K across the turbine stage. A water-cooled Eddy Current Brake (ECB) absorbs the power generated in the turbine rotor. The rotational speed control is as accurate as +/- 1 rpm. Lakshminarayana, Camci, Halliwell, Zaccaria [9] and Town [10] explains the technical characteristics of the rig in detail.

The inlet characteristics of the flow entering the NGV is reported by Town [10]. The Reynolds number of the flow based on the nozzle-exit-velocity and the axial-chord is in the range of 900,000 to 1,000,000. For the rotor, The rotor Reynolds number calculated using the relative inlet velocity is in the range of 250,000 to 450,000. The Reynolds numbers in the turbine stage are representative of a modern HP turbine stage, as explained in Camci [11]. The rotor blades have a span of  $h=123$  mm with the hub to tip ratio of 0.732. The absolute flow exits the rotor blade tip at an angle of 25.160 measured from the axial direction.

**Aerodynamic instrumentation:** The instantaneous performance of the rotor is monitored with an array of Pitot Probes, Kiel Probes, Validyne variable reluctance transducers (DP15), multiplexed differential pressure transducers (ZOC22B/32Px-

2.5psid), Endevco piezoresistive unsteady pressure sensors (8507C-1), and Endevco amplifiers (Model 136).

**Purge flow system:** A 300 psi compressed air system supplies the rim seal cavity purge-flow-generator. The purge injection system used in this study required a few minor modifications to the originally designed purge flow generator by McLean. The general characteristics of this system are described in two papers by McLean, Glezer, and Camci [12], [13]. A flow regulator varies the amount of air being supplied as purge, and an ASME calibrated orifice measures the purge mass flow rate. All data is recorded using scripts through a LabVIEW interface and CompactDAQ data acquisition system from National Instruments. A 16-Bit, 32 channel analog-to-digital converter from National Instruments (NI 9205) is used to acquire signals from the amplifiers and signal conditioners.

**Unsteady pressure measurements in the rim seal cavity:** The structures within the rim seal cavity affect ingress and egress patterns. Previous literature has shown that these structures have an alternating pattern of high and low static pressure. It is possible to calculate the speed and the number of structures present at any given time if at least two fast response probes are held at a known distance apart and can take data simultaneously. Two unsteady transducers manufactured by Endevco (Model 8507C-1) are used to measure the unsteady structures. Figure 2 shows a sketch of the rim seal cavity including a double radial seal. The geometry is classified as a double radial seal. Figure 2 also indicates the radial position of the flush mounted unsteady pressure sensor. The cavity that the red marked transducers in Figure 2 are located next to is referred to as the buffer cavity, it is located between the outer and inner seals. Below the inner seal is a

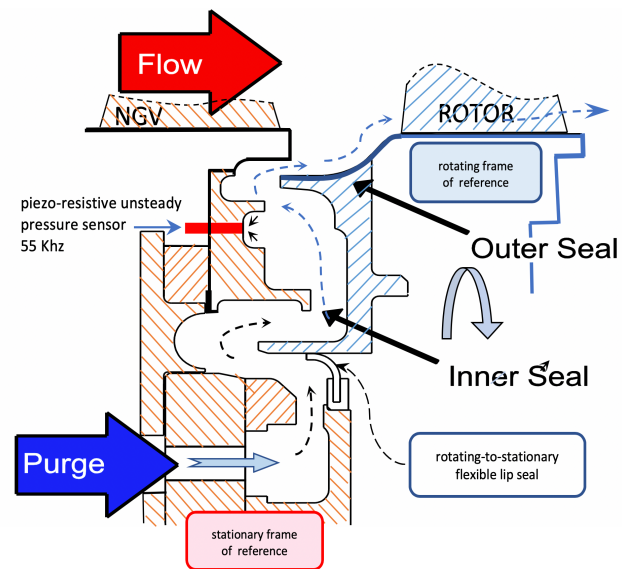


Figure 2 : Rim Seal Cavity Geometry and Unsteady Sensor Location

serpentine path that the injected purge flow must take to the rim seal cavity. This rim seal flow path is designed to fit within our existing experimental rig and is used for flow mixing and settling from the periodic inlets located around the inner perimeter of the annulus. Averbach [14] explains other pertinent details of the rim seal chamber design.

The two pressure transducers are located  $5^\circ$  apart at the same radial position. Figure 3 shows the flush-mounted piezoresistive pressure transducers (Endevco model 8507C-1) that are marked in red colored circular areas. In using our method, at least two probes that can take data simultaneously are necessary to calculate the speed and number of structures within the rim seal cavity.

**Unsteady flow structures in the rim seal cavity:** The unsteady structures in the rim seal cavity each have a unique pressure peak that must shift across the transducers at different times. The modern data acquisition system is set to take data from both piezoresistive pressure probes simultaneously. A prescribed sample rate controlled by the internal clock of the data acquisition device is set so that a time difference can be calculated. The time difference is set by identifying the peak pressure of each unsteady structure and calculating the time difference via the number of samples taken for that peak to pass from one transducer to another. This time difference can be used to calculate the fractional speed at which the structures are moving within the rim seal chamber as shown in Equation (1). In our case,  $\theta_{diff}$  is a known value of  $5^\circ$ .

$$\Omega_{str} = \frac{\theta_{diff}}{360} \frac{2\pi}{t_{phase} \cdot \omega_{rotor}} \quad (1)$$

Unsteady structures will rotate at a fraction of the rotor's angular velocity. Additionally, the number of structures can be obtained by dividing the number of structures that pass by the transducer each second and dividing it by the estimated frequency at which each unique structure passes by the transducer. Equation (2) defines the number of structures as follows:

$$N_{str} = \frac{N_{str \text{ per second}}}{f_{str}} \quad (2)$$

$$N_{str \text{ per second}} = \frac{N_{str \text{ total}}}{T_{sample}}$$

$$f_{str} = \frac{\theta_{diff}}{360} \frac{1}{t_{phase}}$$



Figure 3 : Flush Mounted Piezoresistive Pressure Transducers in Rim Seal Cavity,  $5^\circ$  Apart

## EXPERIMENTAL RESULTS

Table 1 shows the two experimental test cases along with target speed and purge flow rate. The rotor speed is a corrected value based on the current atmospheric temperature. Typically, the laboratory reached thermal equilibrium when the rotor was near 1430 RPM. Purge mass flow injection rate ( $\dot{m}_{purge}$ ) is defined as the mass rate of the fluid being injected into the rim seal cavity externally. Two cases are set, one where no purge flow is used and the rate is at 0.00% of the main gas path flow rate. The target is at 0.25% of the main gas path flow rate. However, a rate of 0.28% was more convenient to set experimentally. Measurements are performed at 100,000 samples per second for 60 seconds to achieve a statistically significant number that can later be compared to the results from the computational RANS based solution.

Table 1

	$RPM_{rotor}$	$\dot{m}_{purge} / \dot{m}_{gaspath}$
Target	1430	0.25% or 0%
Case 1	1433	0.28%
Case 2	1433	0.00%

The test ‘Case 2’, where the purge flow injection rate was held at 0.00% of the inlet mass flow to the turbine, did not produce

results that could be separated from the noise in the signal. As such, the results discussed in this paper will not include ‘Case 2’.

Experimental results are processed in the frequency spectrum. MATLAB employs transformations to convert the pressure signal into the frequency domain using Fast Fourier Transform (FFT) functions. Results are given as a function of occurrences per rotor revolution ( $f^*$ ), the transformation is given below.

$$f^* = \frac{2\pi f}{\omega_{rotor}} \quad (3)$$

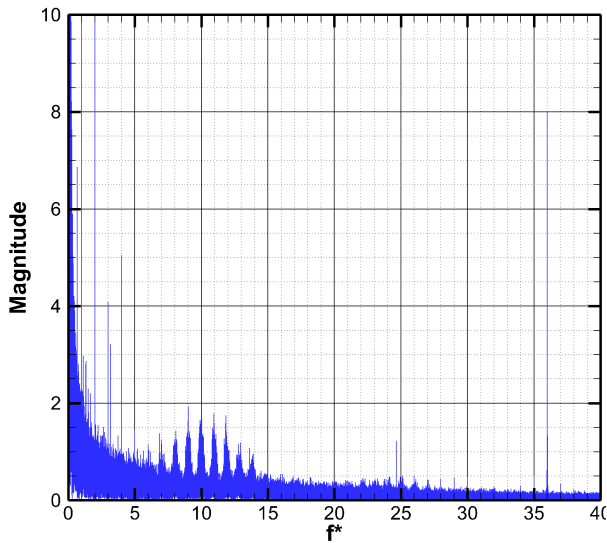


**Figure 4 : FFT of pressure Signals from Transducer 1,  
Case 1 ( $m_{purge}$  is 0.28%)**

The current FFT approach quickly completes the transformations by reducing the complexity of the equation. The fast Fourier transformation is accomplished by adding zeros to the end of the equation until the length is a power of two. The total number of samples for a 60 second run at 100,000 samples per second amounts to 6,000,000 samples. An optimization routine in the current transformation increases the length of the samples to  $2^{23}$ , or 8,388,608 samples.

Figure 4 presents the frequency domain results for a rotor speed of 1433 RPM and a purge mass flow rate of 0.28% of the main gas path for ‘Transducer 1’. A large-magnitude spike is recorded at  $f^* = 36$ . This number is equal to the number of rotor blades and is also the same as the blade-passing-frequency. The results indicate that the transducer is in an area of ingress. Thus, it is more apt to measure the pressure field disturbances caused by the rotor blades as they pass. Frequencies below five occurrences per revolution are understood to be noise.

The second transducer’s frequency spectrum results are shown in Figure 5. The blade passing frequency of 36 is not as pronounced as the first location results. The second transducer is not in a location of constant ingress, and the upstream rotor blade pressure field does not affect it as much. Frequencies below five occurrences per revolution are once again considered noise.

An enlarged version of each graph for the frequency range of 5 to 15 occurrences per revolution is shown in Figure 6. The signals that fall within this range are identified as belonging to the low-frequency, unsteady structures within the rim seal cavity. A range of frequencies is identified as the unsteady structures because the structures may change shape, size, speed, and

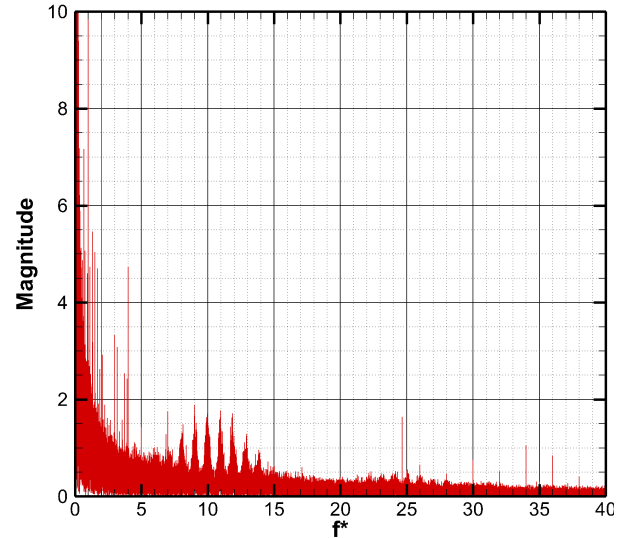


**Figure 5 : FFT of pressure Signals from Transducer 2,  
Case 1 ( $m_{purge}$  is 0.28%)**

periodicity during operation. Additional investigation into how these evolve over time and further analysis of the data will reveal that the structures are unsteady even after a system reaches equilibrium.

A Butterworth type bandpass filter with cutoff frequencies of 5.25 and 16.75 occurrences per revolution is used to isolate the unsteady structure signals from the rest of the measurements. The filtered results of the first case are presented in Figure 7. The signal from ‘Transducer 1’ is in blue on the top, and the signal from ‘Transducer 2’ is in red on the bottom. For ‘Case 1’ a clear set of similar signals is measured by each transducer. The signals are not caused by the blade or vane pressure fields (36 or 29 respectively). They are identified as unsteady flow structures within the rim seal cavity. Calculating the rotational speed and the number of unsteady flow structures is performed by using Equations (1) and (2). What is needed from the filtered data is the number of peaks present in the signal of each

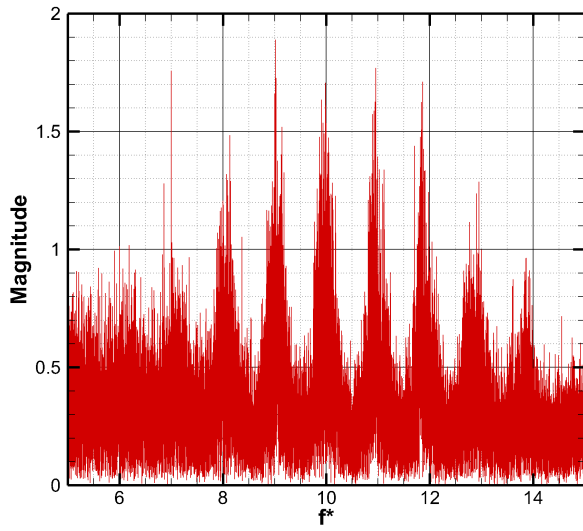
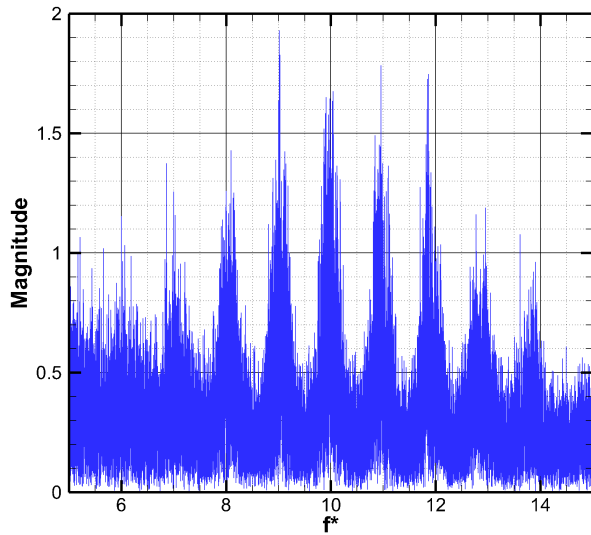


**Figure 6 : Enhanced View of Pressure Signals Transducer 1 (Top, Blue) and Transducer 2 (Bottom, Red)**

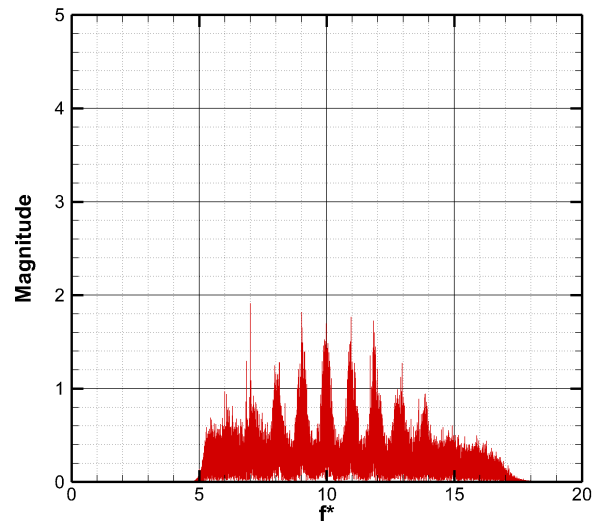
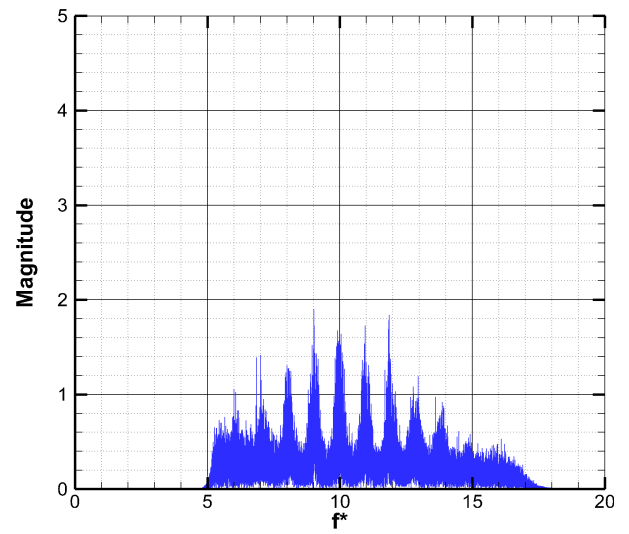


**Figure 7 : Butterworth Bandpass Filtered Pressure Signals Transducer 1 (Top, Blue) and Transducer 2 (Bottom, Red)**

transducer and the time it takes for one peak to traverse between the two transducers. The location and number of peaks are found using the MATLAB function "findpeaks". The function checks to see if a number is higher than a specified range of the immediate numbers around it. The range is set so that the five numbers ahead and behind a value is checked to see which is greater. If the value is greater than all the numbers it is checked against, the value is identified as a peak.

A sample of the data consisting of approximately 20 blade passings is shown in Figure 8. The results show an instantaneous

pressure value subtracted by the average value. The function "findpeaks" identified 16,547 peaks in 'Transducer 1' and 16,585 peaks in 'Transducer 2'.

Identifying the peaks can be used to calculate the time it takes to move from one pressure port to another. The pressure peaks traverse from 'Transducer 1' to 'Transducer 2'. There are 10 microseconds between each sample. Taking the number of samples between each peak and multiplying it by 10 microseconds results in the amount of time it takes for a pressure point

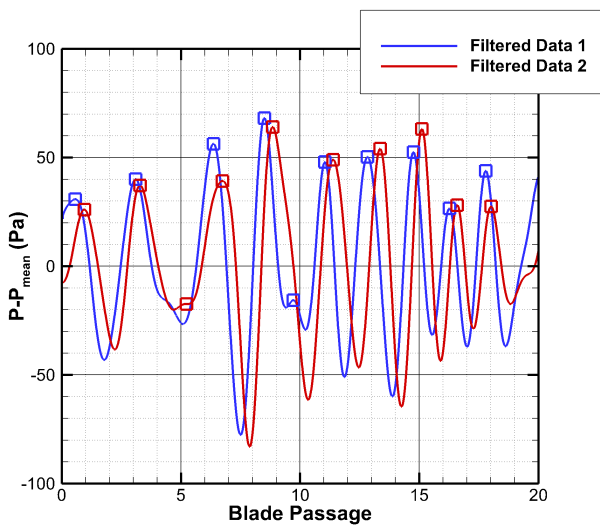


**Figure 8 : Filtered Pressure History with Identified Peaks**

to move between the two transducers.

The current code looks for a pressure peak in the signal of ‘Transducer 1’ when found it calculates the number of samples and the time it takes for the same peak to occur in the signal of ‘Transducer 2’. This calculation is not without flaw. For example, in Figure 8, a peak is identified at 9 blade passings for ‘Transducer 2’. There is not a corresponding peak in the pressure signal for ‘Transducer 2’. The code calculates the time difference between the peak at 9 blade passings from ‘Transducer 1’ and the peak at 13 blade passings from ‘Transducer 2’. This approach creates a large time difference and can skew the results to structures that are measured toward more slowly moving results. The second peak in ‘Transducer 1’ at 13 blade passings also uses the same peak at 13 blade passings in ‘Transducer 2’.

A histogram of the time it takes to traverse from the first transducer to the second is shown in Figure 9. The red represents the average of all the results; it is approximately 1000 microseconds to move between the two transducers. The average results are skewed by the code that cannot account for the missing pressure peaks in the second signal. The mode of the time difference is 750 microseconds. The mode is the value that is used for the calculation of the speed and the number of structures. A more refined code will be able to reduce the data further.

The fractional speed at which the structures are rotating in the rim seal cavity is calculated using Equation (1). The structures are found to be rotating at 77.5% of the rotor speed. This fractional speed is close to the value of 80% reported by Jakoby et al. [2]. It is slower than the rotational speeds recorded by Julien et al. [3] and 87% by Wang et al. [4]. The speed at which the structures rotate is dependent on the geometry of the rim seal cavity and is always recorded as a significant fraction of the rotor speed, but never faster than the rotor rotational speed.

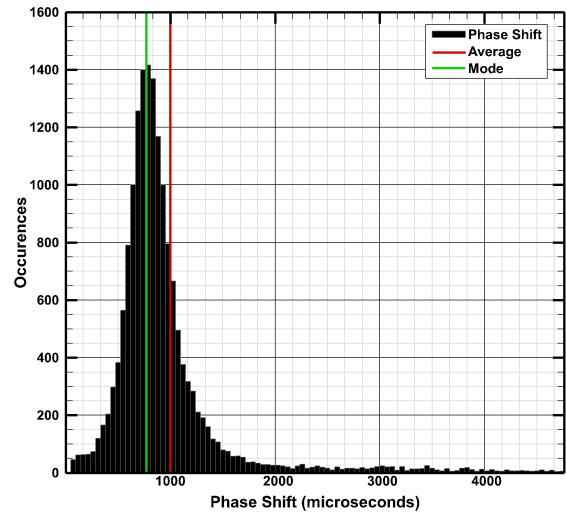


**Figure 9 : Time for an Unsteady Structure to Traverse from Transducer 1 to Transducer 2, Histogram**

Equation (2) determines the number of structures within the rim seal cavity. The number of structures found in the rim seal cavity is calculated to be 14.89, which is rounded up to 15. The number of structures is exceedingly dependent on the geometry of the rim seal cavity. A minimum number of three structures were recorded by Jakoby et al. [2] with a simple axial seal, and a more significant number of 30 structures were recorded by Julien et al. [3].

## COMPUTATIONAL APPROACH

To computationally simulate the flow structures found in the rim seal cavity, ANSYS CFX (64-bit, version 15) is employed as a transient, unsteady, three dimensional, and compressible Reynolds Averaged Navier-Stokes solver. The solver was distributed in parallel mode with as many as 48 licenses used at a time. A similar computational assessment of AFTRF flow using the same computational system is also explained in further detail in Turgut and Camci [15].

Figure 10 shows the geometry representative of the domains in the meridional view. The domain is divided into two subdomains, the first being a stationary domain containing the nozzle guide vane, the stator hub, the casing, and the rim seal cavity. The inlet is located one axial vane cord upstream of the leading edge.

The second domain is the rotating frame of reference and it contains the rotor blade, rotor blade casing, and rotor hub. The exit is located 1.25 blade axial chords downstream of the trailing edge of the rotor blade. The rotational domain is marked with a red boundary.

Stationary surfaces in the figure include the nozzle casing, nozzle hub, stator side of the rim seal cavity, nozzle guide vane surfaces, and rotor casings (green boundary). The rotating surfaces include the rotor hub, rotor casing, rotor blade surfaces (red border). The rotor side of the rim seal cavity is shown in black.

Grid generation was completed with GridPro which creates a multi-block, body-fitted, structured, hexahedral grid and uses automated subroutines to improve mesh quality. Boundary layers are only placed on the hub surfaces and within the rim seal cavity. Boundary layers are not included on the blade or the casing surfaces as they do not have a significant effect on the rim seal cavity ingestion and egression. Additionally, no blade tip clearance gap is used for the rotor.

The size and boundary conditions of the computational domain along with a grid dependency study is recorded in great detail in Averbach [14]. A brief overview of the work will be given here. The computational infrastructure required to complete a full-rotor simulation was not available. There are 29 vanes and 36 blades, a ratio of 0.8056:1. A sector model of 8 vanes and 10 blades is used corresponding to a ratio of 0.8000:1. The calculated pitch ratio between the sector model and the actual stage is 0.9931.

A domain of sufficient size must be used to correctly capture the unsteady structures within the rim seal cavity. From the experimental results, we expect there to be approximately 15 structures. Each structure would be 24° apart from the next structure. The current rim seal cavity simulation contains 99.31° of space and would have the ability to capture 4 of the structures within it.

The unsteady analysis was started by completing a frozen rotor run with stage averaging, which then stepped into the transient simulation. A time step of the required time to move the rotor 1/8th of a blade pitch was chosen, or  $1.4481 \times 10^{-4}$  seconds for the first half of a rotor revolution. Afterward, a finer time step of 1/16th of a blade pitch movement time, or  $7.4405 \times 10^{-5}$  seconds, was used for data gathering. Four blade pitch passages or 64 time steps are completed with 15 inner loops for each time steps. These four-pitch passages are used for transient results.

## COMPUTATIONAL RESULTS

Static pressure in the computational simulation is monitored at the same radial location as the piezoresistive pressure transducers as shown in Figures 2 and 3. Results of the static pressure across the rim seal cavity surface of the first eight vanes are

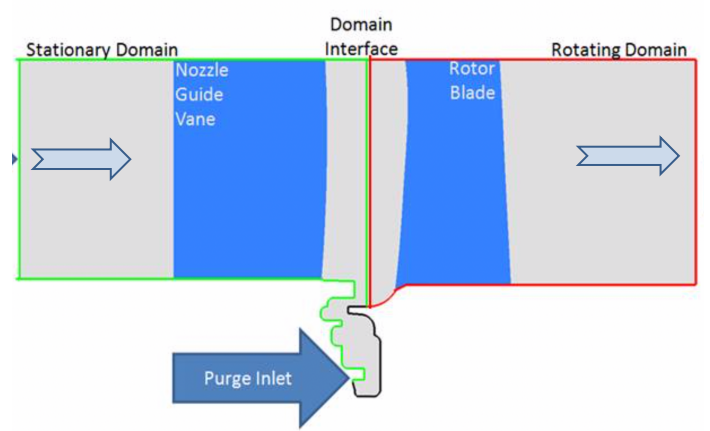


**Figure 10 : Meridional View of the Computational Domain, Stationary Domain (Green), Rotating Domain (Red)**

shown in Figure 11 where a green dot represents a single peak. The red line represents the movement of the rotor. The variable 't' represents the current time, while 'T' represents the time it takes for the rotor to move one blade pitch. At  $t/T=0$  both the green dot and the red line are at the same position. The distance between the green dot and the red line becomes greater as time steps move on. The pressure peak is moving slower than the rotor, as expected. Four pressure peaks are also readily identified in the results. Knowing the numbers of the vanes in the domain (8) and the number of the vanes in the full stage (29) makes it possible to find the total number of structures in the computationally simulated turbine stage. The current calculation shows that in the simulated stage there are 14.5 unsteady structures.

$$\Omega_{str} = \frac{\theta_{peak,t+1} \theta_{peak,t}}{\omega_{rotor} \Delta t} \frac{\pi}{180} \quad (4)$$

The speed at which the structures rotate can be calculated using Equation (4). The rotor speed, along with the time step, is set with the initial conditions of the simulation. The four peaks observed in Figure 11 are mapped for the time step and recorded in Figure 12. The figure shows the rotor moving (black dot-dash line) at a constant speed which is greater than the speed of all peaks. The four peaks do not move uniformly and have variance in speed from one step to another. The peaks could be inherently unsteady, or an insufficient number of rotor rotations were used during the simulation before data is collected. The authors' opinion is that the structures are, and will continue to be, unsteady during the simulation. The average speed for which the peaks are moving is 81.7% of the rotor speed. This is also the rotational speed at which the unsteady structures are moving.

**Table 2: Results of Experimental and Computational Analysis of Unsteady Cells within the Rim Seal Cavity**

	Experimental	CFD
<b>Number of Cells</b>	15	14.5
<b>Cell Speed/Rotor Speed</b>	77.5%	81.7%

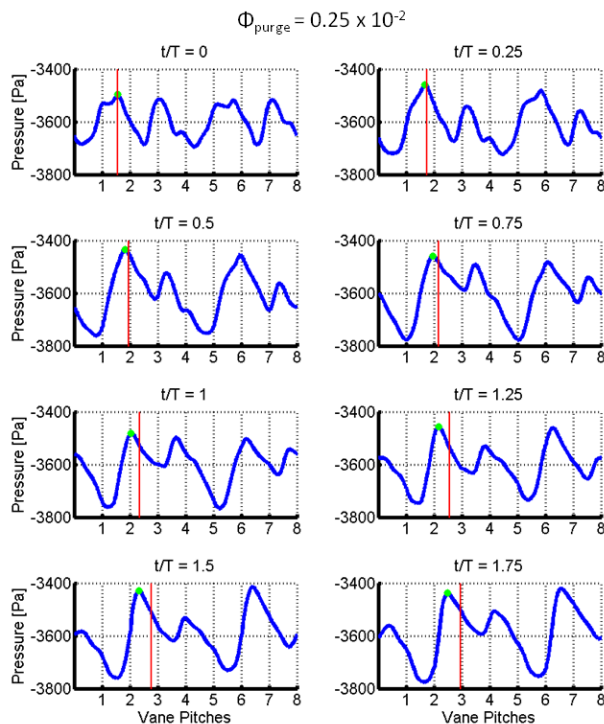


**Figure 11 : Static Pressure Across the NGV Side Rim Seal Cavity at Varying Time**

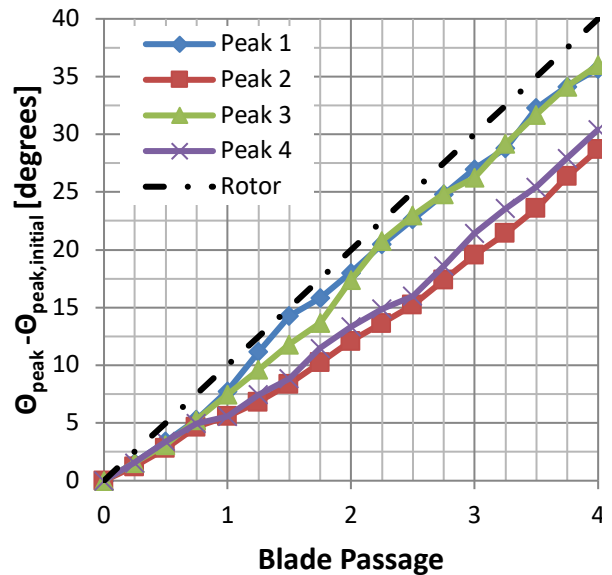


**Figure 12 : Static Pressure Peak Location**

The number of cells is due to the way the rim seal cavity is dependent on the number of vanes used in the simulation (8) and the total number of vanes in the stage (29). There are a prime number of vanes which helps to eliminate vibrations in the system at the cost of increased complexity for the computational analysis.

The structures in the rotor are measured experimentally to be moving at 77.5% rotor speed, while the structures in the computational study are found to be moving at 81.7% rotor speed. The computational fractional speed results of the cavity flow structures are found to be within a good agreement with the current turbine stage experiments.

The computational results would benefit from a full rotor simulation with an increased number of revolutions during the transient phase. The larger domain would allow more structures to develop. The increased number of revolutions would allow the structures to develop more and settle.

The experimental results would benefit from increased scrutiny into the measured data sets. The averaged results compare favorably to the URANS code. However, URANS by definition will average, the structures may be inherently unsteady and could not ever settle down to a steady state solution.

## CONCLUSIONS

A test to compare the experimental and computational results for the fractional speed of the rim seal cavity flow structures is proposed and executed. To the authors' knowledge, there has been no such experimental analysis using piezoresistive pressure transducers to investigate unsteady cells within the rim seal cavity.

A more in-depth look into the results from the piezoresistive transducers may reveal that the structures are changing in size, shape, and periodicity even after steady state operation of the turbine has been reached.

## ACKNOWLEDGMENTS

The authors would like to thank Özhan Turgut for his guidance in computational meshing and CFD operation. Harry Houtz and Nick Doroschenko is acknowledged for their expertise in all things related to the unsteady probe and mechanical, systems. The authors are also indebted to NASA NRA program and Pratt and Whitney Aircraft Engines for the minor modifications of the existing rim seal chamber of AFTRF.

## REFERENCES

1. C. Cao, J. W. Chew, P. R. Millington and S. I. Hogg, 2003, "Interaction of Rim Seal and Annulus Flows in an Axial Flow Turbine," in *Proceedings of the ASME Turbo Expo 2003*, Atlanta.
2. R. Jakoby, T. Zierer, K. Lindblad, J. Larsson, L. deVito, D. E. Bohn, J. Funcke and A. Decker, 2004, "Numerical Simulation of the Unsteady Flow Field in an Axial Gas Turbine Rim Seal Configuration," in *ASME IGTI 2004-53829*, Vienna,
3. S. Julien, J. Lefrancois, G. Dumas, G. Boutet-Blais, S. Lapointe, J.-F. Caron and R. Marini, 2010, "Simulations of Flow Ingestion and Related Structures in a Turbine Disk Cavity," in *ASME IGTI 2010*, Glasgow.
4. C.Z. Wang, B. V. Johnson, S. P. Mathiyalagan, J. A. Glahn and D. F. Cloud, 2012, "Rim Seal Ingestion in a Turbine Stage from 360-Degree Time-Dependant Numerical Simulations," in *ASME IGTI2012-6*, Copenhagen.
5. A.V. Mirzamoghadam, S. Kanjiyani, A. Riahi, R. Vishnumolakala and L. Gundeti, 2014, "Unsteady 360 CFD Validation of a Turbine Stage Mainstream/Disc Cavity Interaction," in *ASME IGTI2014-25466*, Dusseldorf.
6. P. Palafox, Z. Ding, J. Bailey, T. Vanduser, K. Kirtley, K. Moore and R. Chupp, "A New 1.5-Stage Turbine Wheelspace Hot Gas Ingestion Righ (HGIR) - Part I: Experimental Test Vehicle, Measurement Capability and Baseline Results,", 2013, in *ASME IGTI2013-96020*, San Antonio.
7. A. M. Basol, A. Raheem, M. Huber and R. S. Abhari, 2014, "Full-Annular Numerical Investigation of the Rim Seal Cavity Flows Using GPU's," *ASME IGTI2014-26755*, Dusseldorf.
8. P. Palafox, Z. Ding, K. Moore, R. Chupp and K. Kirtley, 2013, "A New 1.5-Stage Turbine Wheelspace Hot Gas Ingestion Rig (HGIR) - Part II: CFD Modeling and Validation," in *ASME IGTI2013-96021*, San Antonio.
9. Lakshminarayana, B., Camci, C., Halliwell, I., Zaccaria, M., 1996, "Design, Development, and Prediction of a Turbine Research Facility to Study Rotor Stator Interaction Effects," *Int. Journal of Turbo and Jet Engines*, **13**, pp. 155-172.
10. J. Town , 2015, "An Investigation of Rim Seal/Disk Cavity Flow and its Interaction with High Pressure Turbine Rotor Flows," Ph.D. Thesis, 2015d, The Pennsylvania State University.
11. C. Camci, 2004, "A Turbine Research Facility to Study Tip Desensitization Including Cooling Flows," *VKI Lecture Series on "Turbine Blade Tip Design and Tip Clearance Treatment"*, 1-26.
12. C. McLean, C. Camci and B. Glezer, 2001, "Mainstream Aerodynamic Effects Due to Wheelspace Coolant Injection in a High-Pressure Turbine Stage: Part I- Aerodynamic Measurements in the Stationary Frame," *Transactions of the ASME, Journal of Turbomachinery*, Vol. 123, no. 4, pp. 687-696.
13. C. McLean, C. Camci and B. Glezer, 2001, "Mainstream Aerodynamic Effects due to Wheel Space Coolant Injection in a High Pressure Turbine Stage, Part-II Rotational Frame Measurements," *Transactions of the ASME, Journal of Turbomachinery*, Vol. 123, no. 4, pp. 697-703.
14. M. Averbach, 2014, "Simulation and Experimental Validation of the Wheel Space of the Axial Flow Turbine Research Facility Under Low Purge Flow Conditions," Master of Science Thesis, The Pennsylvania State University The Graduate School.
15. Turgut, Ö. H., & Camci, C., 2016, "Factors Influencing Computational Predictability of Aerodynamic Losses in a Turbine Nozzle Guide Vane Flow," *Journal of Fluids Engineering*, **138**(5), 051103-051103-051113.  
doi:10.1115/1.4031879